How Si affects the microstructural evolution and phase transformations of intermetallic γ-TiAl based alloys

Michael Musi, Benjamin Galy, Andreas Stark, Norbert Schell, Muriel Hantcherli, Jean-Philippe Monchoux, Alain Couret, Helmut Clemens, Petra Spoerk-Erdely

How Si affects the microstructural evolution and phase transformations of intermetallic γ-TiAl based alloys

Michael Musi[a,*], Benjamin Galy[b], Andreas Stark[c], Norbert Schell[c], Muriel Hantcherli[b], Jean-Philippe Monchoux[b], Alain Couret[b], Helmut Clemens[a], Petra Spoerk-Erdely[a]

[a] Department of Materials Science, Montanuniversität Leoben, Franz Josef-Straße 18, 8700 Leoben, Austria
michael.musi@unileoben.ac.at (Michael Musi), helmut.clemens@unileoben.ac.at (Helmut Clemens), petra.spoerk-erdely@unileoben.ac.at (Petra Spoerk-Erdely)

[b] Centre d'Élaboration de Matériaux et d'Etudes Structurales (CEMES), CNRS, BP 94347, 29 rue Jeanne Marvig, 31055 Toulouse, France
benjamin.galy@cemes.fr (Benjamin Galy), muriel.hantcherli@cemes.fr (Muriel Hantcherli) monchoux@cemes.fr (Jean-Philippe Monchoux), alain.couret@cemes.fr (Alain Couret)

[c] Institute of Materials Research, Helmholtz-Zentrum Hereon, Max-Planck-Straße 1, 21502 Geesthacht, Germany
andreas.stark@hereon.de (Andreas Stark), norbert.schell@hereon.de (Norbert Schell)

* Corresponding author:
Email: michael.musi@unileoben.ac.at (Michael Musi)
Telephone: +4338424024204

Abstract

Small additions of Si and C have been proven to efficiently improve the creep properties of intermetallic γ-TiAl based alloys. In order to exploit the full potential of these alloying elements, detailed studies of their influence on the phase transformations and the resulting microstructural evolution during processing and heat treatments are a necessity. This work presents a fundamental investigation of the alloying effect of Si in the composition range up to 0.65 at.% on a β-solidifying TiAl alloy with the nominal composition of Ti-43.5Al-4Nb-1Mo-0.1B (in at.%). After casting and a subsequent heat treatment at 1200 °C, Si increases the amount of γ phase at the expense of the α_2-Ti_3Al phase. Due to solid solution strengthening and the precipitation of ζ-Ti_5Si_3 silicides in the highly Si-alloyed materials, an increase in hardness is observed. As the silicides act as effective obstacles for grain boundaries, these precipitates also control the grain growth kinetics of the α phase and are able to maintain a fine-grained microstructure at 1300 °C for holding times up to 20 h. By utilizing in-situ high-energy X-ray diffraction experiments and differential scanning calorimetry, Si is found to exhibit similar effects as Al on the alloying system, effectively increasing solid-solid phase transition temperatures, while simultaneously decreasing the solidus temperature of the materials.

Keywords: Titanium aluminides, Microstructure, Phase transformations, High-energy X-ray diffraction, Transmission electron microscopy (TEM)

1. Introduction

In order to reduce the emission of harmful greenhouse gases, the aircraft and automotive industries require innovative high-temperature materials to improve engine efficiency [1,2]. An outstanding class of alloys meeting the challenging requirements, i.e. high creep resistance and low density for the application as low pressure turbine blades, are intermetallic γ-TiAl based alloys, which possess only half the density of currently used Ni-base alloys [3–5]. The suitability of γ-TiAl based alloys as creep-exposed materials in aircraft engines has already been proven by their incorporation in the latest engine families of several manufacturers, e.g. General Electrics and Safran Aircraft Engines [1,4]. A γ-TiAl based alloy belonging to the 4th alloy generation is the so-called TNM alloy (Ti-43.5Al-4Nb-1Mo-0.1B, in at.%). This alloy, in particular, is characterized by excellent mechanical properties balanced between sufficient room temperature ductility on one hand and high creep resistance on the other hand [3,5,6]. As its alloying concept relies on the addition of Nb and Mo, i.e. elements that stabilize the disordered body-centred cubic (bcc) β phase (A2, *Im-3m*), the phase transformation behaviour of this alloy is heavily altered compared to the binary Ti-Al system [3,7–9]. At room temperature, the TNM alloy consists of the ordered tetragonal face-centred γ-TiAl phase ($L1_0$, *P4/mmm*), the ordered hexagonal α_2-Ti_3Al phase ($D0_{19}$, *P6$_3$/mmc*) and the ordered bcc β_o phase (B2, *Pm-3m*) [3,4,10]. The latter is the ordered counterpart of the high-temperature β phase [3,6]. Above the eutectoid temperature, the hexagonal phase is present in its disordered form, the so-called α phase (A3, *P6$_3$/mmc*) [4,10]. Various additional phases, e.g. ω_o and ω", can also be found in the microstructure, depending on the thermal history of the material [11].

In the search of further improvement of the creep resistance of γ-TiAl based alloys to broaden their application portfolio, several alloying concepts utilizing different additional elements have been in the focus of research in the past decades [3,12,13]. A promising candidate to enhance the creep resistance of γ-TiAl based alloys is Si [14–17]. In addition to its beneficial influence

on the oxidation resistance, small quantities result in a substantial strengthening of the material by pronounced solid solution hardening in its role as substitutional element [18–21]. Due to interfacial drag mechanisms, Si-containing alloys are characterized by a higher thermal stability of the lamellar α_2/γ colonies, which are beneficial for creep applications [14,22,23]. Alloying with Si in quantities above the constitution-depending solubility limit of the alloy results in the formation of ζ-Ti_5Si_3 silicides ($D8_8$, *P6₃/mcm*) [10,24,25]. As observed by Noda et al. [24] in a Ti-48Al-1.5Cr-0.65Si (in at.%) alloy, the silicide formation can occur in a eutectic ($L \rightarrow \beta+\zeta$-$Ti_5Si_3$) as well as a eutectoid ($\alpha_2 \rightarrow \gamma+\zeta$-$Ti_5Si_3$) way. The latter one is observed for many Si-bearing γ-TiAl based alloys during creep, occurring in the vicinity of α_2/γ colonies [13,15,26,27]. These silicides form especially at the α_2/γ lamellar interface due to the eutectoid nature of their formation, consequently hindering dislocation motion by decorating γ-(111) planes and thus increasing the creep resistance [14]. For γ-TiAl based alloys containing β-stabilizing elements, such as Nb, Mo and W, the formation of silicides inside the β_o phase rather than within the α_2/γ colonies has also been reported [16,25].

In order to combine the beneficial influence of Si and C on the mechanical properties with the hot workability of the TNM alloy, which exceeds that of many other γ-TiAl based alloys due to the presence of β phase at forging temperatures, the so-called TNM+ alloy has been developed [6,13,28]. The constitution of this alloy is characterized by additions of 0.3 at.% C and 0.3 at.% Si as well as a reduced Al content to compensate for the α-stabilizing effect of C [28]. However, even alloying of such low quantities of C and Si can be expected to induce a significant alteration of the phase fraction evolution and transition temperatures. In a detailed study of the effect of C on the TNM alloy, Schwaighofer et al. [29] have shown that already small additions of C can result in the stabilization of an α single phase field region at high temperatures and change the solidification behaviour of the material from β-solidification to a peritectic one. With respect to Si, a knowledge gap regarding its effect on the microstructure

evolution during processing and phase transformations of β-solidifying γ-TiAl based alloys is found in literature.

The present work aims at closing this gap by studying the effect of Si on a fundamental basis in several γ-TiAl alloys based on the TNM alloying concept. Specifically, alloys with nominal Si content of 0.25 at.%, 0.45 at.% and 0.65 at.% as well as a conventional TNM alloy are investigated in different stages of processing. The conducted characterization of phase distribution, hardness and the size of microstructural constituents after solidification and a subsequent heat treatment, which resembles the thermal history of hot-isostatic pressing (HIP), highlights the influence of Si on the microstructural evolution. As the presence of silicides is confirmed by complementary experimental techniques in the course of this work, their effect on the grain coarsening behaviour of the α phase in the range of typical heat treatment temperatures was investigated and evaluated with respect to Zener drag and Ostwald ripening. In-situ high-energy X-ray diffraction (HEXRD) heating experiments as well as differential scanning calorimetry (DSC) were employed to determine the effect of Si on the occurring phases and their transformations. In combination with additional heat treatment studies, these techniques give insight into the phase transitions, correlating with the change of the microstructural properties, and allow for the first time the establishment of a quasi-binary phase diagram for TNM-based alloys in dependence of the Si content.

2. Material and methods

This work investigates four alloys based on the TNM alloying concept: a conventional TNM alloy and three alloys with different amounts of Si. In accordance with their nominal Si contents in at.%, these alloys are designated TNM-0.25Si, TNM-0.45Si and TNM-0.65Si. The exact alloy compositions are given in Table 1. They were determined by X-ray fluorescence spectroscopy and inductively coupled plasma atomic emission spectroscopy. The amount of O,

which was measured by carrier gas hot extraction, is below 1000 m.-ppm for all alloys. The alloys were provided by GfE Metalle und Materialien GmbH, Nuremberg, Germany, in the form of four times remelted cast buttons produced from pre-alloyed starting material. This material condition will be referred to as the "as-cast" state. The as-cast material was exposed to a heat treatment at 1200 °C for 4 hours followed by furnace cooling performed in a calibrated high-temperature furnace of the type RHF 1600 from Carbolite, Germany. This temperature profile corresponds to a typical HIP process, which is conducted on γ-TiAl based alloys to achieve better chemical homogeneity, to bring the material closer to thermodynamic equilibrium and to close residual casting porosity [3]. This material condition, designated henceforth as "HIP heat-treated", was the starting condition for the further conducted experiments and heat treatments.

Table 1. Chemical composition of the investigated TNM-based alloys containing different concentrations of Si.

Alloy	Chemical composition [at.%]					
	Ti	Al	Nb	Mo	B	Si
TNM	bal.	43.85	3.80	0.96	0.09	0.03
TNM-0.25Si	bal.	43.93	3.81	0.95	0.1	0.23
TNM-0.45Si	bal.	43.81	3.86	0.96	0.09	0.44
TNM-0.65Si	bal.	43.91	3.90	0.98	0.09	0.65

Microstructural investigations of the alloys at different length scales were performed by light optical microscopy (LOM), scanning electron microscopy (SEM) and transmission electron microscopy (TEM). For LOM and SEM, the samples were mechanically ground and polished. Details on the metallographic preparation procedure can be found in Ref. [30]. LOM was performed on an AxioImager.M2 LOM from Zeiss, Germany. Micrographs of the microstructure were taken by SEM in back-scattered electron (BSE) mode with a field-emission device Versa 3D Dual Beam from Thermo Fisher, USA, operating at an acceleration voltage of

20 kV. Image analysis of SEM-BSE micrographs using the software Stream Motion from Olympus Soft Imaging Solutions, Germany, was used to determine the size of the α_2/γ colonies in the as-cast and HIP heat-treated condition. The field-emission device Versa 3D Dual Beam was further equipped with a Hikari XP electron back-scatter diffraction (EBSD) camera from EDAX, USA, which was used to quantify the α grain size of material exposed to grain coarsening heat treatments at 1300 °C for various holding times under normal atmosphere followed by water-quenching in the above-mentioned high-temperature furnace. For EBSD data acquisition and evaluation, the softwares TEAM and OIM, both from EDAX, USA, were used. TEM samples of the different material conditions were prepared according to the procedure described in Ref. [31]. Microstructural characterization by TEM was carried out on a Jeol 2010 from Jeol, Japan, using an acceleration voltage of 200 keV. Chemical analysis of large microstructural constituents, i.e. lamellar α_2/γ colonies, was performed by energy dispersive X-ray spectroscopy (EDS) on a SEM of type CLARA from Tescan, Czech Republic, equipped with an 80 mm^2 X-max detector and the software Aztec from Oxford Instruments, United Kingdom. Hardness measurements of the HIP heat-treated material condition were performed on a Qness Q 60 A+ measuring device equipped with a Vickers indenter tip. For each alloy, 10 individual measurements were performed.

The influence of Si on the occurring phases and their transformations was investigated by in-situ HEXRD and DSC. The in-situ HEXRD heating experiments were conducted at the Hereon-operated beamline P07 at PETRA III at the Deutsches Elektronen-Synchrotron (DESY), Hamburg, Germany. The synchrotron radiation beam had a mean photon energy of 73.6 keV, corresponding to a wavelength of 0.16859 Å, and a cross-section of 1×1 mm^2. For each HIP heat-treated alloy, a cylindrical specimen with a diameter of 5 mm and a length of 10 mm was heated in a modified DIL805A/D dilatometer from TA Instruments, Germany, by an induction coil in a high-purity Ar atmosphere [32]. The sample temperature was measured by

a thermocouple of type S. A Ta foil with a thickness 0.2 mm, which was spot-welded to the sample, acted as a diffusion barrier. The used temperature profile consisted of an isothermal holding segment at 1000 °C, which lasted for 15 min and was followed by a heating segment up to 1400 °C with a heating rate of 2 °C/min. This slow heating rate was employed to measure the volume fractions of the occurring phases close to thermodynamic equilibrium. Complete Debye-Scherrer diffraction rings were captured during the in-situ HEXRD heating experiments with a XRD 1621 area detector from Perkin Elmer, USA, positioned centrally at a distance of 1500 mm behind the samples. The diffraction setup was calibrated using LaB_6 as reference material and the obtained 2D diffraction data were azimuthally integrated with the software Fit2D [33]. The quantification of the volume fractions and lattice parameters of the individual phases as a function of temperature was performed by Rietveld analysis of the integrated data using the software MAUD [34]. DSC was conducted on a LabsysEvo from Seteram, France, using cylindrical samples of HIP heat-treated material with a mass of 80 mg. The samples were heated in Al_2O_3 crucibles closed with an Al_2O_3 cap in Ar atmosphere during the measurement. For each alloy, three different heating rates, i.e. 10, 20, and 40 °C/min, were applied to determine the phase transition temperatures of solid-solid transformations up to 1400 °C in thermodynamic equilibrium by extrapolation of the measured values to a heating rate of 0 °C/min. Phase transformations at higher temperatures, e.g. close to the solidus temperature, were derived from experiments performed with a heating rate of 20 °C/min up to 1550 °C. The phases present at temperatures above the range of the in-situ HEXRD experiments were determined from heat treatments at 1425 °C and 1450 °C for 20 min followed by water-quenching using the high-temperature furnace described above. Additional heat treatments were conducted at 1300 °C for 1 h followed by gas-quenching in a DIL805A from TA Instruments, Germany, in a high-purity Ar atmosphere in order to prevent any influence of O.

3. Results and discussion

3.1. Effect on microstructural evolution

The as-cast microstructures of the TNM, TNM-0.25Si, TNM-0.45Si and TNM-0.65Si alloy are presented in the form of SEM-BSE micrographs in Figs. 1a-d, respectively. The main microstructural constituents are marked by white arrows. In general, no pronounced elemental segregation occurred due to a solidification pathway that proceeded completely via the β phase [35]. All alloys consist of lamellar α_2/γ colonies with a columnar shape surrounded by β_o phase. In the latter one, small γ platelets formed during cooling. The elongated shape of the α_2/γ colonies, which is typical of moderate cooling rates, is attributed to the morphology of the high-temperature α phase formed via the incomplete ($\beta \rightarrow \alpha$) transformation during solidification according to the Burgers orientation relationship [10]. Due to the addition of B, Ti-borides are found in all as-cast microstructures. While they yield a grain-refining effect during solidification due to enhanced heterogeneous nucleation, no influence of B on the phase transformations can be expected [36,37]. The presence of low quantities of silicides in the vicinity of the boundaries of the α_2/γ colonies can be confirmed for the TNM-0.45Si and TNM-0.65Si alloy. A corresponding SEM image of an example is shown in the insert of Fig. 1d. As these silicides can be expected to be of type ζ-Ti_5Si_3, they exhibit the brightest contrast in the composition-sensitive SEM-BSE micrograph [25]. Although the TNM-0.45Si and TNM-0.65Si alloy possess relatively high Si contents compared to other alloys studied in the past [13,25], no silicides are observed by SEM in the α_2/γ colonies themselves. This may correlate with the fact that silicides typically precipitate in this specific microstructural constituent during prolonged thermal exposure, e.g. creep [14,15], and that their formation kinetics were insufficient for the occurring cooling rate of the casting process used in this study.

As-cast material was heat treated at 1200 °C for 4 hours followed by furnace cooling, which corresponds to the temperature profile of a HIP processing typically performed for γ-TiAl based

alloys to close casting porosity and bring the material closer to thermodynamic equilibrium [3]. The resulting microstructures in this HIP heat-treated condition are shown in Figs. 1e-h and are identical with conventional HIP material [38]. Generally, compared to the as-cast microstructures, a coarsening of the α_2/γ colonies as well as of the γ lamellae themselves is caused by the HIP heat treatment. A comparison of the α_2/γ colony shapes reveals a difference between the alloys. While a globularization of the colonies occurred for the TNM and the TNM-0.25Si alloy, the pronounced columnar shape of the colonies is still immanent for the other two alloys. At the colony borders, the γ platelets were replaced by globular γ phase. With respect to the silicides, precipitation in different parts of the microstructure is observed in the TNM-0.45Si and TNM-0.65Si alloy. Firstly, silicides are present inside the α_2/γ colonies in the HIP heat-treated condition, in contrast to the as-cast material. A comparison between a silicide-free colony in the TNM alloy and a silicide-containing colony in the TNM-0.65Si alloy, as presented in Fig. 2a and Fig. 2b, shows that these elongated silicides are predominately observed at lamellae interfaces. Thus, it is tempting to speculate that they have formed by the eutectoid transformation $\alpha_2 \rightarrow \gamma+\zeta\text{-}Ti_5Si_3$ as reported by Noda et al. [24] and Tsuyama et al. [26], i.e. by nucleating at α_2/γ interfaces and growing into α_2 lamellae [27]. The silicides observed in the colonies in the TNM-0.45Si alloy evidence that their absence in the as-cast condition is related to insufficient formation kinetics. Secondly, the majority of the silicides precipitated in the globular γ phase formed during the HIP-heat treatment. Thirdly, a minor amount of silicides has formed in the β_o phase, mostly at its borders with other microstructural constituents, i.e. α_2/γ colonies and globular γ phase. Examples for the latter two types of silicides can be seen in Fig. 2c, which reveals a globular morphology. Their precipitation is caused by the formation of globular γ phase possessing a low solubility for Si, which also explains why the majority of silicides formed at the colony borders is present in the vicinity of this phase [39].

The influence of Si on different microstructural properties is summarized in Fig. 3. The size distributions of the α_2/γ colonies in the as-cast and HIP heat-treated alloys are displayed in Fig. 3a. The colony area was determined by image analysis of SEM-BSE micrographs. With increasing Si content, the size of the colonies is found to decrease in the as-cast material. As mentioned above, the size of the α_2/γ colonies corresponds to the size of the α grains formed during solidification and the subsequent phase transformations. Due to the higher Si solubility of the β phase when compared to the α phase, this element enriches in the β phase during the ($\beta \rightarrow \alpha$) transformation, creating a force counteracting the grain growth of the α phase by solute drag and, thus, reducing its grain size [25]. The shift of the curves in Fig. 3a after the HIP-heat treatment denotes a coarsening of the colonies. However, the shift of all curves by approximately the same value indicates that the effect of Si during the heat treatment is negligible. As the temperature of the HIP-heat treatment, i.e. 1200 °C, is situated within the ($\alpha+\beta_o+\gamma$) phase field region, see the TNM phase diagram reported in Ref. [38], the present phases, i.e. the β_o phase situated at the colony borders, dictate the coarsening behaviour of the α_2/γ colonies.

Figure 3b shows the room temperature HEXRD spectra for the TNM-0.65Si alloy in the as-cast and HIP heat-treated material condition. In addition to peaks of the various TiAl-related phases, peaks belonging to the crystal structure of the ζ-Ti_5Si_3 silicides are also observed (green diamonds). By means of Rietveld analysis of the HIP heat-treated diffraction spectrum, the lattice parameters of the ζ-Ti_5Si_3 silicides were determined to be a=7.542 Å and c=5.217 Å. These values are in good agreement with literature. Sun et al. [22], for example, reported for a Ti-48Al-3Si alloy (in at.%) after a heat treatment at 1200 °C for 12 hours followed by air cooling lattice parameter values of a=7.527 Å and c=5.250 Å, respectively, as measured by X-ray diffraction. The slight differences probably arise from the fact that ζ-Ti_5Si_3 silicides contain certain amounts of Nb in TNM-based alloys [25]. A comparison between the as-cast

and the HIP heat-treated material condition further reveals, on the one hand, a shift of the diffraction peaks of all phases related to the transition towards thermodynamic equilibrium during the HIP-heat treatment as well as elemental redistribution, and, on the other hand, a change of the relative peak intensities indicating an adjustment of their respective volume fractions [3].

For the quantification of these volume fractions, also Rietveld analysis was utilized. The resulting phase distribution in the as-cast and HIP heat-treated condition for all four alloys is displayed in Fig. 3c. Alloying with Si causes an increasing amount of γ phase at the expense of α_2 phase, while the amount of β_o phase is unaffected in the as-cast condition. The observed increase in γ phase is in accordance with observations from literature [21,24,26], e.g. with the transformation pathway $\alpha_2+\gamma \rightarrow \alpha_2+\gamma+\zeta\text{-}Ti_5Si_3 \rightarrow \gamma+\zeta\text{-}Ti_5Si_3$ for an increasing Si content as reported by Tsuyama et al. [26]. As the area fraction of the α_2/γ colonies, the β_o phase and the γ platelets, determined by image analysis of the same SEM-BSE micrographs used for Fig. 3a, are constant for alloys in the as-cast condition, the higher amount of γ phase for the Si-alloyed materials can only be explained by an increased fraction of γ phase inside the colonies. The HIP-heat treatment results in a further shift of the phase distribution in the direction of the γ phase. As this increase is the same for all alloys, i.e. approximately 5 vol.%, this effect is not caused by Si, but rather by the HIP-heat treatment itself. This additional increase in γ phase is associated primarily with the formation of globular γ phase at the colony borders as their relative fraction in the HIP heat-treated microstructure is significantly higher when compared to the one of the γ platelets in the as-cast condition.

With respect to the silicides, HEXRD revealed their presence in the as-cast condition only for the TNM-0.65Si alloy. However, as mentioned above, some silicides could be observed in the as-cast TNM-0.45Si alloy by means of SEM, meaning that their volume fraction was just too low to be detected by HEXRD. After the HIP-heat treatment, an increase in their volume

fraction can be observed. Thus, in the HIP heat-treated material condition, silicide peaks were also observed for the TNM-0.45Si alloy because of the increased amount of γ phase compared to the as-cast condition. This increased amount of silicides is found at the borders of the α_2/γ colonies, where the globular γ phase forms during the HIP-heat treatment. As this phase has the lowest solubility for Si, an increase of its phase fraction yields a decreasing overall Si solubility of the alloy itself [25]. The formation of silicides inside the α_2/γ colonies during the HIP-heat treatment is related to kinetic reasons, as the cooling rates during solidification prevented their formation.

A lower bound for the Si solubility can be derived from the volume fractions presented in Fig. 3c and the work by Klein et al. [25], who determined the Si contents of the α_2, β_o and γ phase for a C- and Si-containing TNM-based alloy by means of atom probe tomography. In the case of the TNM-0.25Si alloy in the HIP heat-treated condition, the corresponding Si solubility limit is estimated as 0.288 at.%, which explains why no silicides are observed. This value agrees with findings in literature: the TNM+ alloy containing 0.3 at.% Si, for example, exhibits a solubility limit of 0.29 at.% due to slightly different phase fractions and, thus, shows precipitation of silicides after HIP [13]. For the TNM-0.45Si alloy, the estimated Si solubility of 0.281 at.% is lower compared to the TNM-0.25Si alloy due to a higher amount of γ phase. Thus, approximately 0.15 at.% Si should be insolvable in said alloy. As the Si content of the silicides in TNM-based alloys is only around 20 at.% due to incorporation of Nb and Al [25], the undissolved Si should yield slightly below 1 vol.% of silicides, which is in good agreement with the experimentally determined value of 1.5 vol.% in the HIP heat-treated condition.

In order to predict the effect of Si on the material's strength, the hardness of the alloys in the HIP heat-treated condition was determined. As depicted in Fig. 3d, the hardness increases with increasing Si content. However, in contrast to a continuous increase, a discontinuity in the hardness curve is observed between 0.25 and 0.45 at.% Si. Generally, the hardness depends on

a variety of different composition and microstructure-specific properties. However, most of these properties are either continuously changing with the Si content or do not depend on it at all. Exemplary for the first case are the colony size, the corresponding phase distribution and the Si content present in the α_2/γ colonies, the most dominant microstructural constituent. Their Si content was determined by EDS measurements, see Fig. 3d. Essentially, it indicates an increased solute solution hardening due to a higher concentration of dissolved Si, which has also been reported in literature [13,21]. A microstructural property, which is obviously independent of the Si concentration, is the average lamellae width of the α_2/γ colonies, which was found to be in the range of 115±45 nm for all alloys by means of TEM. The only contribution, which can cause such a discontinuity in hardness, are the silicides present only in the TNM-0.45Si and TNM-0.65Si alloy in the different parts of the microstructure. Consequently, this means that the increased hardness of the TNM-0.45Si and the TNM-0.65Si alloy can be attributed to both solid solution strengthening and precipitation hardening due to the addition of Si.

3.2. Effect on grain coarsening

Advanced γ-TiAl based alloys destined for applications at elevated temperatures are desired to possess a fully lamellar microstructure only consisting of α_2/γ colonies to achieve extraordinary creep resistance [3]. This requires heat treatments in the phase field region above the dissolution temperature of the γ phase, where typically solely the α phase is present for many γ-TiAl based alloys, and, thus, causes extensive and undesired grain growth [3,10]. In section 3.1., Si was found to be capable of effectively reducing the grain growth even if present only as a solute. In order to study the influence of silicides on the grain coarsening behaviour of the α phase, the alloys were subjected to heat treatments for various holding times at 1300 °C, which is above the γ-solvus temperature of all investigated alloys (see section 3.3.). These heat treatments were

followed by water-quenching to avoid the formation of γ phase and allow the characterization of the high-temperature microstructure. It should be noted that while the γ formation is suppressible, the ordering of the α phase, present during the heat treatment, into the α_2 phase cannot be avoided by water-quenching [40].

After a holding time of 10 min, small amounts of β_o phase can still be found in the microstructure, as shown exemplarily in Fig. 4a for the TNM alloy. In the higher Si-containing alloys, the TNM-0.45Si and TNM-0.65Si alloy precisely, the silicides are present in the form of a network situated at the boundaries of the α grains, while the silicides existing inside the former colonies have completely dissolved. A comparison between the microstructure of the TNM and the TNM-0.65Si alloy, as presented in Fig. 4a, gives first indications of the significant effect of the silicides on the resulting α grain size.

Increased heat treatment times result in the occurrence of discontinuous grain growth in the TNM, TNM-0.25 and TNM-0.45Si alloy, as evidenced in Fig. 4b. This type of grain growth is often observed for materials that contain a growth-inhibiting second phase. Due to differences in size and spatial distribution of the second phase, heat treatments in the range of its dissolution temperature can result in the observed bimodal grain size distribution caused by discontinuous grain growth [41,42]. In the present case, a discrimination has to be made between the TNM, TNM-0.25 and TNM-0.45Si alloy with respect to this second phase. For the first two alloys, the β_o phase, which dissolves due to O pick-up during the heat treatments, triggers the discontinuous grain growth after approximately 15 min, whereas in the case of the TNM-0.45Si alloy the silicides are responsible for this effect [10]. However, the time after which this coarsening phenomenon occurs is increased to 150 min in the latter alloy. As there are still silicides present after the 150 min heat treatment (see insert in Fig. 4b), the reason for the discontinuous grain growth is related to their coarsening, the accompanied reduction in number and the loss of pinning effect on the grain boundaries.

Contrarily, the TNM-0.65Si alloy, containing a higher amount of silicides, still shows a fine α grain size even after a heat treatment for 20 h, as evidenced by the inverse pole figure map determined by EBSD presented in Fig. 4c. However, due to the spatial distribution of the silicides, which resembles the columnar form of the α_2/γ colonies in the as-cast condition, the α grains possess an elongated shape as microstructural globularization was also hindered by the silicides. In order to evaluate the grain growth kinetics of the TNM-0.65Si alloy, a model as formulated by Eq. 1 was used, which assumes the migration of curved grain boundaries towards their centre of curvature [43,44]:

$$D^n - D_0^n = K * t. \qquad \text{(Eq. 1)}$$

Here, D and D_0 denote the grain size after a given time t and at the beginning, respectively. The value n is known in literature as the time exponent and K is a constant factor. Fitting this model to the grain size values obtained by EBSD for different heat treatment times, yields the results presented in Fig. 4d. An excellent accordance between this theoretical model and the experimental data points is found. For the time exponent n, a value of 3.41 was determined for the coarsening in the α single phase field region. This is in accordance with literature, as the theoretical value for this parameter should be between 3 and 4 depending on the occurring type of diffusion [45]. Additionally, due to an expected linear dependence between the grain size D and the size of the silicides for a constant volume fraction of silicides, whose coarsening behaviour is governed by Ostwald ripening exhibiting a time exponent of 3, the obtained value for n is not surprising [41,46]. Furthermore, Morris et al. [44] investigated the grain coarsening behaviour in the (α+γ) two-phase field region of a Ti-48Al-2Mn-2Nb-0.06C (in at.%) alloy and observed a similar value for n between 2.5 and 3 due to the presence of α globules and carbides at the grain boundaries.

In Fig. 5, a TEM bright field micrograph of a silicide precipitate after a heat treatment time of 20 h is shown, including the corresponding qualitative EDS mappings for the relevant alloying

elements. The lens-like morphology is in contrast to the shape of the silicides in the HIP heat-treated condition (compare Fig. 2c and Fig. 5) and is typical of grain boundary-pinning precipitates, where an equilibrium of the different interfacial energies has been reached [41,47,48]. The EDS mappings in Fig. 5 show that the silicide contains an increased amount of Ti, Nb, Mo and Si, while the Al content is lower compared to the surrounding α_2 grains. Quantitative measurements yielded a mean composition of the silicides of 49.9 at.% Ti, 25.3 at.% Si, 15.9 at.% Al, 7.4at.% Nb, and 1.5 at.% Mo. Generally, this result is in agreement with the findings of Klein et al. [25], who also reported an enrichment of Al and Nb in ζ-Ti_5Si_3 silicides. Small deviations in the exact values might arise from differences in the experienced thermal history and measuring techniques in comparison to Ref. [25].

3.3. Effect on phase transformations

Although the additions of Si to the TNM alloying system are below 1 at.% in the present work, the change of the phase distribution in the as-cast and HIP heat-treated conditions indicates a significant influence of this element on the occurring phase transformations. A powerful tool for time-resolved investigations of such transformations in intermetallic γ-TiAl based alloys is in-situ HEXRD [49]. Combined with Rietveld analysis, this method grants valuable insights into the evolution of the volume fractions and lattice parameters of the occurring phases.

In the present work, HIP heat-treated material was heated from 1000 °C up to 1400 °C employing a heating rate of 2 °C/min to ensure that the measured volume fractions correspond closely to thermodynamic equilibrium. The resulting phase fraction evolution for the investigated alloys is show in Fig. 6a. As the heating to 1000 °C has little influence on the phase fractions, the values at 1000 °C correspond to the phase distribution presented in Fig. 3c. Temperatures up to 1100 °C only result in a slight decrease in the amount of γ phase. At temperatures between 1150 °C and 1200 °C, the α_2 phase disorders into the α phase at the

eutectoid temperature. For exact values the reader is referred to the phase diagram shown in Fig. 10 at the end of this chapter and Table A.1 in the appendix. During further heating, a significant increase in the α fraction mostly at expense of the γ phase occurs until the latter one has completely dissolved at the γ-solvus temperature and a maximum of α phase is present within the samples. Regarding the β_o phase, the volume fraction increases to a local maximum in the temperature range of 1150 °C to 1200 °C. Disordering into the β phase occurs in the temperature interval from 1200 °C to 1250 °C. After a decline into a minimum between 1225 °C and 1300 °C, depending on the alloy variant, a significant increase in the β phase fraction at the expense of the α phase is observed. Due to the high temperatures, extensive grain coarsening occurs in the TNM and TNM-0.25Si alloy, which is evident from the increased scattering of the related curves. Consequently, while the observed trends are still reasonable for temperatures above 1325 °C, the exact volume fractions are questionable.

The results for the TNM alloy are in accordance with previous measurements performed by Schwaighofer et al. [38]. Small differences, e.g. with respect to the slightly higher γ-solvus temperature, can be explained by the higher Al content of the investigated material compared to the material investigated in Ref. [38]. The additions of Si shift the characteristic features of the phase evolution, e.g. dissolution of the γ phase, maximum in the amount of α phase and minimum in β phase, to higher temperatures and increase the amount of γ phase at the expense of the α/α_2 phase as reported in literature [26]. Above the γ-solvus temperature, Si tends to stabilize the α phase over β, as the volume fraction of the former phase is higher at a given temperature for the Si-containing alloys.

The ζ-Ti_5Si_3 silicides observed in the TNM-0.45Si and TNM-0.65Si alloy are found to be stable up to temperatures above 1350 °C. To better visualize the evolution of their volume fraction compared to the other phases, Fig. 6b presents the relative intensity evolution of the ζ-Ti_5Si_3-002 peak and the γ-200 peak of the TNM-0.65Si alloy. During the decline of the γ peak,

the silicide peak decreases accordingly. This can be attributed to the dissolution of the silicides inside the α_2/γ-colonies, which is in agreement with the water-quenched microstructure after a heat treatment at 1300 °C for 10 min (see Fig. 4a), i.e. just above the γ-solvus temperature, as well as with results from literature, e.g. the phase transformation $\gamma+\zeta\text{-}Ti_5Si_3 \rightarrow \alpha_2$ during heating [24,26]. The significant dissolution of silicides indicated by the pronounced decline of the silicide peak above the γ-solvus temperature is caused by the increasing amount of β phase, whose solubility for Si is higher compared to the α phase [25]. Thus, the Si solubility effectively increases because of the transformation from α to β during heating. Consequently, a lower dissolution temperature of the silicides is observed for the TNM-0.45Si alloy when compared to the TNM-0.65Si alloy, as the amount of β phase present at a given temperature is higher in the former one.

Rietveld analysis of the HEXRD data also reveals the evolution of the lattice parameters of the TiAl-related phases, i.e. α/α_2, β/β_o and γ, which is shown exemplarily for the TNM-0.65Si alloy in Fig. 7. Generally, the changes of the *c/a* ratio of the different phases are related to changes of the respective phase composition [50,51]. The visualization via the *c/a* ratio has been chosen for the α/α_2 (c/a_{hex}) and γ phase (c/a_{γ}) in order to compensate for most of the effects arising from thermal expansion, while for the β/β_o phase the lattice parameter (a_{bcc}) is shown because of the cubic crystal structure [10]. Note that the *c/a* ratios of the α and α_2 phase have been calculated with respect to the crystal structure of the disordered α phase.

At temperatures below 1150 °C, only minor changes are observed in accordance with the phase fraction evolution, as diffusion is limited. The significant decline of c/a_{hex} just below 1200 °C corresponds to the disordering reaction $\alpha_2 \rightarrow \alpha$. The following dissolution of the γ phase (see Fig. 6a) causes a continuous decrease of c/a_{hex} and increase of c/a_{γ} due to the redistribution of elements, i.e. mostly Al, according to the alloy's phase diagram [51]. A similar behaviour has also been reported for other γ-TiAl based alloys [50,51]. In the case of the β/β_o phase, the

influence of thermal expansion on the lattice parameter a_{bcc} is the only observable effect until 1200 °C. The first deviation from the almost linear thermal expansion behaviour is associated with the disordering transformation of β_o into β. The decline of the amount of β phase up until 1300 °C causes a further deviation of a_{bbc} from the linear expansion behaviour. As the β volume fraction decreases to a minimum in the course of the heating experiment, this phase enriches in the β-stabilizing elements Nb and Mo [10,52–54]. The increase in β phase above 1300 °C and the elemental exchange with the α phase result in an increase of a_{bcc} as well as of c/a_{hex}. Generally, the above described phenomena are qualitatively the same for the other alloys, only shifted to lower temperatures due to the lower Si content.

The minimum in the amount of β phase in the temperature range of 1225 °C to 1300 °C is known in literature and is one key point of the success of the TNM alloying concept, as it allows to minimize the β amount present in the final microstructure by special heat treatments [3,5]. However, for the heat treatments performed at this temperature in the course of the grain coarsening study, a dissolution of the β phase was observed in all alloys. As their increased Al content of 43.9 at.% might give rise to an α single phase field region, e.g. see Ref. [38], the question arises if this minimal amount of β is real for all alloys or if this phase is only observed in the in-situ HEXRD heating experiments due to a combination of the applied heating rate and slow dissolution kinetics, i.e. involving the low diffusivity of Nb and Mo enriched in the β phase [55].

To answer this question, heat treatments were performed at 1300 °C for 1 h followed by Ar gas-quenching in a high-purity Ar atmosphere to prevent any influence from the α-stabilizing O, which always occurs when heat treatments are conducted in air [4]. The resulting microstructures are presented in Figs. 8a-d. Although the transformation of the β phase into the α phase cannot be suppressed by water-quenching [40], the differentiation between the high-temperature α phase and β phase can still be made by the different chemical composition and

morphology of the high-temperature α phase and the α_2 laths formed from the β phase during water-quenching. These lath-like structures in Fig. 8 reveal the presence of β phase in all alloys and, consequently, prove the existence of the (α+β) phase field region in all investigated alloys. Furthermore, the decreasing amount of β phase with respect to the Si content is in agreement with the observed phase evolution in Fig. 6a. These findings imply that the β phase must be stable for the heat treatments performed in the course of the grain coarsening study. However, due to its generally very low fraction in the TNM-0.65Si alloy at 1300 °C (< 2 vol.%) and the fact that it dissolves in less than 20 min due to the influence of O, no effect on the results for the TNM-0.65Si alloy, i.e. the evaluation of the α grain growth kinetics (Fig. 4d), can be expected as the shortest heat treatment time used for the model (Eq. 1) was 50 min.

A complementary assessment of the phase transition temperatures in the temperature range of the in-situ HEXRD heating experiments as well as of the ones occurring at higher temperatures, e.g. melting of the alloys, was performed by DSC. Several distinct peaks associated with the occurring phase transformations can be observed in the related curves for a heating rate of 20 °C/min as shown in Fig. 9a. Starting at low temperatures, the first peak (1) corresponds to the eutectoid transformation, which partially overlaps with the peak of the dissolution of the γ phase (2). The eutectoid and γ-solvus temperature have been determined by extrapolation of temperatures measured at three heating rates (10, 20 and 40 °C/min) to a heating rate of 0 °C/min, i.e. thermodynamic equilibrium. Above 1400 °C, i.e. the maximum temperature of the in-situ HEXRD heating experiments, the peak of the $\alpha \rightarrow \beta$ phase transformation (3) is observed. Generally, all peaks and, consequently, the phase transformations are in good accordance with the phase evolution determined by means of in-situ HEXRD. The highest peak (5), which is only partially visible in Fig. 9a as the strong rise of the heat flow at the highest temperatures, belongs to the melting of the materials, i.e. representing the $\beta \rightarrow L$ transformation.

Interestingly, due to the alloying with Si, an additional peak (4) occurs just before this melting peak. Since silicides were found to dissolve at lower temperatures during the in-situ HEXRD heating experiments, this peak cannot be related to any transformations involving silicides. Therefore, as it can only be caused by transformations between the α, the β and the liquid phase, this peak belongs to the peritectic transformation, which during heating reverses to $\alpha \rightarrow \beta+L$ [4,38]. To investigate the possible presence of α phase at temperatures just below the corresponding peak, which arises as a necessity for the occurrence of this peak, heat treatments were performed on the TNM and TNM-0.65Si alloy at 1425 °C and 1450 °C for 20 min followed by water-quenching. The resulting microstructures are shown in Fig. 9b. The differentiation between the high-temperature α phase and β phase is the same as for Fig. 8. At a temperature of 1425 °C, both α and β phase can be found in the TNM and TNM-0.65Si alloy. For the latter one, a lower amount of α_2 laths, caused by a lower amount of β phase, is present, which, in accordance with the results of the in-situ HEXRD heating experiments shown in Fig. 6a, confirms the shift of the $\alpha \rightarrow \beta$ transformation to higher temperatures because of the Si additions. The results of the heat treatments at 1425 °C also show that the maximum peak temperature corresponding to the $\alpha \rightarrow \beta$ transformation in the DSC curves (Fig. 9a) underestimates the real transition temperature, as remnants of the high-temperature α phase can still be found in the microstructure. After a heat treatment at 1450 °C, a microstructure consisting only of α_2 laths, formed via the transformation of the β phase, is observed in the TNM alloy as well as in the TNM-0.65Si alloy. Thus, it can be concluded that a β single phase field region is present at high temperatures for all of the investigated alloys, which is in accordance with literature for the TNM alloy [3,38]. Furthermore, this confirms that the peritectic peaks observed for the Si-containing alloys in the DSC curves (Fig. 9a) are measurement artefacts and only occur due to insufficient dissolution kinetics of the α phase caused by the applied heating rate of 20 °C/min. The increase of the peritectic peaks' height with respect to the Si addition is caused by the shift of the $\alpha \rightarrow \beta$ transformation to higher

temperatures, narrowing the time window for dissolution of α and, consequently, making a higher amount of this phase available for this non-equilibrium peritectic transformation. The absence of this peritectic reaction in thermodynamic equilibrium is further confirmed by the as-cast microstructures (Fig. 1), which are free of any pronounced segregations, as it is typical of alloys solidifying completely via the β phase [35].

The results of the in-situ HEXRD and DSC experiments as well as of the heat treatments can be combined to assess a quasi-binary phase diagram based on the TNM alloying concept for the first time in dependence of the Si content. The resulting diagram is shown in Fig. 10. For the exact phase transition temperatures, the reader is referred to Table A.1 in the appendix. As indicated by the phase evolution and DSC measurements, alloying with Si yields an increase of the temperatures of solid-solid phase transformations, e.g. $\gamma \rightarrow \alpha$ and $\alpha \rightarrow \beta$. Contrarily, for the phase transition involving the liquid phase, i.e. $\beta \rightarrow L$, a decreasing temperature is observed, effectively narrowing the β single phase field region at high temperatures with increasing Si content. Thus, the effect of Si is comparable to the one of Al with respect to the phase transformations in the investigated composition range of γ-TiAl based alloys [38]. Consequently, it can be expected that through alloying with Si in sufficient quantities higher than 0.65 at.%, a peritectic transformation may occur in thermodynamic equilibrium, similar to the Ti-Al system [9]. With respect to the phase transformation pathway occurring during cooling, a change from $L \rightarrow \beta+L \rightarrow \beta \rightarrow \alpha+\beta \rightarrow \alpha+\beta+\gamma \rightarrow \alpha+\beta_o+\gamma \rightarrow \alpha+\alpha_2+\beta_o+\gamma \rightarrow \alpha_2+\beta_o+\gamma$ to $L \rightarrow \beta+L \rightarrow \beta \rightarrow \alpha+\beta \rightarrow \alpha+\beta+\zeta\text{-}Ti_5Si_3 \rightarrow \alpha+\beta+\gamma+\zeta\text{-}Ti_5Si_3 \rightarrow \alpha+\beta_o+\gamma+\zeta\text{-}Ti_5Si_3 \rightarrow \alpha+\alpha_2+\beta_o+\gamma+\zeta\text{-}Ti_5Si_3 \rightarrow \alpha_2+\beta_o+\gamma+\zeta\text{-}Ti_5Si_3$ is caused by sufficient additions of Si. The lower boundary for the stability region of $\zeta\text{-}Ti_5Si_3$ (see circle 1 in Fig. 10) was chosen in accordance with the Si content of the TNM+ alloy, i.e. 0.3 at.%, for which the presence of $\zeta\text{-}Ti_5Si_3$ silicides has been confirmed in HIP material [13]. In comparison to C, which represents another important alloying element of the TNM+ alloy added to improve the creep strength, the effect

involving the liquid phase is similar, as C additions also result in the occurrence of a peritectic transformation [13,29]. However, while C is known as a strong α-stabilizing element, Si was found in the present study to preferably stabilize the γ phase over the α and α_2 phase in accordance with previous observation from literature [26,29].

4. Conclusions

Four intermetallic TNM-based alloys with Si contents of 0 at.%, 0.25 at.%, 0.45 at.%, and 0.65 at.% were investigated in the present study regarding the influence of Si on the microstructural evolution during processing and heat treatments as well as on the occurring phase transformations. Alloying with Si results in the stabilization of the γ phase over the α_2 phase after casting and a heat treatment simulating the HIP process. Furthermore, the size of the α_2/γ colonies is reduced. Sufficient Si contents yield the precipitation of ζ-Ti_5Si_3 silicides, containing certain amounts of Al and Nb, inside all microstructural constituents, i.e. lamellar α_2/γ colonies, globular γ phase and β_o phase. Due to a simultaneous contribution of solid solution strengthening and precipitation hardening, Si improves the hardness of the investigated alloys. During heat treatments at 1300 °C, the silicides act as effective obstacles for the grain boundaries, therefore, limiting pronounced α grain growth, if present in sufficient quantities. The coarsening kinetics of the α grains are directly related to the coarsening of the silicides and, thus, evolve with a time exponent similar to Ostwald ripening. With respect to the influence on the phase fractions and transition temperatures, Si exhibits a similar effect as Al in the investigated composition range, essentially, increasing the amount of the γ phase and at the expense of the α_2 phase below the γ-solvus temperature and shifting solid-solid phase transformations like the transition of $\alpha \rightarrow \beta$ to higher temperatures. With respect to the solid-liquid transition, i.e. $\beta \rightarrow L$, a decreasing solidus temperature is caused by alloying with Si.

Ultimately, the obtained results allow the establishment of a quasi-binary phase diagram for TNM-based alloys in dependence of the Si content for the first time.

Acknowledgements

This research was funded in part by the Austrian Science Fund (FWF) [Project Number I 3932-N36]. For the purpose of open access, the author has applied a CC BY public copyright licence to any Author Accepted Manuscript version arising from this submission. Michael Musi is a Recipient of a DOC Fellowship of the Austrian Academy of Sciences at the Department of Materials Science, Montanuniversität Leoben. We acknowledge DESY (Hamburg, Germany), a member of the Helmholtz Association HGF, for the provision of experimental facilities. Parts of this research were carried out at beamline P07 at PETRA III. Beamtime was allocated for proposal I-20200691 EC.

Appendix

Table A.1 summarizes the phase transition temperatures determined by means of in-situ HEXRD, DSC and heat treatments (HT). Note that the DSC results correspond to transition temperatures determined by an extrapolation of the measured temperatures to a heating rate of 0 °C/min. The accuracy of the determined transition temperatures is within ±5 °C.

Table A.1. Phase transition temperatures in °C of the investigated alloys.

Alloy	$(\alpha_2 \rightarrow \alpha)_{Start}$		$(\alpha_2 \rightarrow \alpha)_{End}$	$\beta_o \rightarrow \beta$	γ-solvus		ζ-solvus	β-transus	Solidus
	HEXRD	DSC	HEXRD	HEXRD	HEXRD	DSC	HEXRD	DSC+HT	DSC
TNM	1148	1151	1165	1198	1268	1261	-	1435	1512
TNM-0.25Si	1155	1157	1182	1212	1279	1272	-	1438	1503
TNM-0.45Si	1160	1162	1190	1218	1291	1281	1373	1441	1494
TNM-0.65Si	1171	1167	1197	1219	1293	1285	1395	1445	1484

References

[1] B.P. Bewlay, S. Nag, A. Suzuki, M.J. Weimer, TiAl alloys in commercial aircraft engines, Mater. High Temp. 33 (2016) 549–559.

[2] B.P. Bewlay, M.J. Weimer, T. Kelly, A. Suzuki, P.R. Subramanian, The science, technology, and implementation of TiAl alloys in commercial aircraft engines, Mater. Res. Soc. Sym. Proc. 1516 (2013) 49–58.

[3] H. Clemens, S. Mayer, Design, processing, microstructure, properties, and applications of advanced intermetallic TiAl alloys, Adv. Eng. Mater. 15 (2013) 191–215.

[4] F. Appel, H. Clemens, F.D. Fischer, Modeling concepts for intermetallic titanium aluminides, Prog. Mater. Sci. 81 (2016) 55–124.

[5] S. Mayer, P. Erdely, F.D. Fischer, D. Holec, M. Kastenhuber, T. Klein, H. Clemens, Intermetallic β-solidifying γ-TiAl based alloys − From fundamental research to application, Adv. Eng. Mater. 19 (2017) 1600735.

[6] H. Clemens, W. Wallgram, S. Kremmer, V. Guether, A. Otto, A. Bartels, Design of novel β-solidifying TiAl alloys with adjustable β/B2-phase fraction and excellent hot-workability, Adv. Eng. Mater. 10 (2008) 707–713.

[7] H. Chladil, H. Clemens, Zickler, Gerald, A., M. Takeyama, E. Kozeschnik, A. Bartels, T. Buslaps, R. Gerling, S. Kremmer, L.A. Yeoh, K.-D. Liss, Experimental studies and thermodynamic simulation of phase transformations in high Nb containing γ-TiAl based alloys, Int. J. Mat. Res. 98 (2007) 1131–1137.

[8] S. Mayer, C. Sailer, H. Nakashima, T. Schmoelzer, T. Lippmann, P. Staron, K.-D. Liss, H. Clemens, M. Takeyama, Phase equilibria and phase transformations in molybdenum-containing TiAl alloys, Mater. Res. Soc. Sym. Proc. 1295 (2011) 113–118.

[9] J.C. Schuster, M. Palm, Reassessment of the binary aluminum-titanium phase diagram, J. Phase Equilibria Diffus. 27 (2006) 255–277.

[10] F. Appel, J.D.H. Paul, M. Oehring, Gamma titanium aluminides - science and technology, WILEY-VCH, Weinheim, 2011.

[11] M. Schloffer, B. Rashkova, T. Schoeberl, E. Schwaighofer, Z. Zhang, H. Clemens, S. Mayer, Evolution of the ω_o phase in a β-stabilized multi-phase TiAl alloy and its effect on hardness, Acta Mater. 64 (2014) 241–252.

[12] A. Couret, J.-P. Monchoux, D. Caillard, On the high creep strength of the W containing IRIS-TiAl alloy at 850 °C, Acta Mater. 181 (2019) 331–341.

[13] M. Kastenhuber, B. Rashkova, H. Clemens, S. Mayer, Enhancement of creep properties and microstructural stability of intermetallic β-solidifying γ-TiAl based alloys, Intermetallics 63 (2015) 19–26.

[14] Y.-W. Kim, S.-L. Kim, Effects of microstructure and C and Si additions on elevated temperature creep and fatigue of gamma TiAl alloys, Intermetallics 53 (2014) 92–101.

[15] A. Dlouhý, K. Kuchařová, Creep and microstructure of near-gamma TiAl alloys, Intermetallics 12 (2004) 705–711.

[16] J. Lapin, T. Pelachová, M. Dmoánková, D. Daloz, M. Nazmy, Influence of long-term creep exposure in the mircrostructure stability of cast Ti-46Al-2W-0.5Si alloy for turbine blades, Kovove Mater. 45 (2007) 121–128.

[17] C. Zhou, F.P. Zeng, B. Liu, Y. Liu, K. Zhao, J. Lu, C. Qiu, J. Li, Y. He, Effects of Si on microstructures and high temperature properties of beta stabilized TiAl alloy, Mater. Trans. 57 (2016) 461–465.

[18] S. Taniguchi, K. Uesaki, Y.-C. Zhu, Y. Matsumoto, T. Shibata, Influence of implantation of Al, Si, Cr or Mo ions on the oxidation behaviour of TiAl under thermal cycle conditions, Mater. Sci. Eng. A 266 (1999) 267–275.

[19] B.G. Kim, G.M. Kim, C.J. Kim, Oxidation behavior of TiAl-X (X=Cr, V, Si, Mo or Nb) intermetallics at elevated temperature, Scripta Metall. Mater. 33 (1995) 1117–1125.

[20] Y. Shida, H. Anada, The effect of various ternary additives on the oxidation behavior of TiAl in high-temperature air, Oxid. Met. 45 (1996) 197–219.

[21] S.W. Kim, P. Wang, M.H. Oh, D.M. Wee, K.S. Kumar, Mechanical properties of Si- and C-doped directionally solidified TiAl–Nb alloys, Intermetallics 12 (2004) 499–509.

[22] F.-S. Sun, S.-E. Kim, C.-X. Cao, Y.-T. Lee, M.-G. Yan, A study of Ti_5Si_3/γ interface in TiAl alloys, Scripta Mater. 45 (2001) 383–389.

[23] R. Yu, L.L. He, J.T. Guo, H.Q. Ye, V. Lupinc, Orientation relationship and interfacial structure between ζ-Ti_5Si_3 precipitates and γ-TiAl intermetallics, Acta Mater. 48 (2000) 3701–3710.

[24] T. Noda, M. Okabe, S. Isobe, M. Sayashi, Silicide precipitation strengthened TiAl, Mater. Sci. Eng. A 192–193 (1995) 774–779.

[25] T. Klein, B. Rashkova, D. Holec, H. Clemens, S. Mayer, Silicon distribution and silicide precipitation during annealing in an advanced multi-phase γ-TiAl based alloy, Acta Mater. 110 (2016) 236–245.

[26] S. Tsuyama, S. Mitao, K. Minakawa, Alloy modification of γ-base titanium aluminide for improved oxidation resistance, creep strength and fracture toughness, Mater. Sci. Eng. A 153 (1992) 451–456.

[27] P.I. Gouma, M. Karadge, In situ observation of carbide and silicide precipitation in C+Si alloyed γ-TiAl, Mater. Lett. 57 (2003) 3581–3587.

[28] E. Schwaighofer, H. Clemens, J. Lindemann, A. Stark, S. Mayer, Hot-working behavior of an advanced intermetallic multi-phase γ-TiAl based alloy, Mater. Sci. Eng. A 614 (2014) 297–310.

[29] E. Schwaighofer, B. Rashkova, H. Clemens, A. Stark, S. Mayer, Effect of carbon addition on solidification behavior, phase evolution and creep properties of an intermetallic β-stabilized γ-TiAl based alloy, Intermetallics 46 (2014) 173–184.

[30] C. Fleissner-Rieger, T. Pogrielz, D. Obersteiner, T. Pfeifer, H. Clemens, S. Mayer, An additively manufactured titanium alloy in the focus of metallography, Pract. Metallogr. 58 (2021) 4–31.

[31] T. Voisin, J.-P. Monchoux, M. Perrut, A. Couret, Obtaining of a fine near-lamellar microstructure in TiAl alloys by Spark Plasma Sintering, Intermetallics 71 (2016) 88–97.

[32] P. Staron, T. Fischer, T. Lippmann, A. Stark, S. Daneshpour, D. Schnubel, E. Uhlmann, R. Gerstenberger, B. Camin, W. Reimers, E. Eidenberger, H. Clemens, N. Huber, A. Schreyer, In situ experiments with synchrotron high-energy X-rays and neutrons, Adv. Eng. Mater. 13 (2011) 658–663.

[33] A.P. Hammersley, S.O. Svensson, M. Hanfland, A.N. Fitch, D. Hausermann, Two-dimensional detector software: From real detector to idealised image or two-theta scan, High Pressure Res. 14 (1996) 235–248.

[34] L. Lutterotti, Total pattern fitting for the combined size–strain–stress–texture determination in thin film diffraction, Nucl. Instrum. Meth. B 268 (2010) 334–340.

[35] V. Kuestner, M. Oehring, A. Chatterfee, H. Clemens, F. Appel, Analysis of the solidification microstructure of multi-component gamma titanium aluminide alloys, in: D.M. Herlach (Ed.), Solidification and crystallization, WILEY-VCH, Weinheim, 2004, pp. 250–258.

[36] D. Hu, Role of boron in TiAl alloy development: a review, Rare Met. 35 (2016) 1–14.

[37] U. Hecht, V. Witusiewicz, A. Drevermann, J. Zollinger, Grain refinement by low boron additions in niobium-rich TiAl-based alloys, Intermetallics 16 (2008) 969–978.

[38] E. Schwaighofer, H. Clemens, S. Mayer, J. Lindemann, J. Klose, W. Smarsly, V. Guether, Microstructural design and mechanical properties of a cast and heat-treated intermetallic multi-phase γ-TiAl based alloy, Intermetallics 44 (2014) 128–140.

[39] P.I. Gouma, M.J. Mills, Y.-W. Kim, Characterization of the precipitation process in a TiAl-based alloy with carbon and silicon additions, Philos. Mag. Lett. 78 (1998) 59–66.

[40] K.-D. Liss, A. Bartels, H. Clemens, S. Bystrzanowski, A. Stark, T. Buslaps, F.-P. Schimansky, R. Gerling, C. Scheu, A. Schreyer, Recrystallization and phase transitions in a γ-TiAl-based alloy as observed by ex situ and in situ high-energy X-ray diffraction, Acta Materialia 54 (2006) 3721–3735.

[41] G. Gottstein, Physical foundations of materials science, Springer, Berlin, 2001.

[42] F.J. Humphreys, A new analysis of recovery, recrystallisation, and grain growth, Mater. Sci. Technol. 15 (1999) 37–44.

[43] A.K. Jena, M.C. Chaturvedi, Phase transformations in materials, Prentice Hall, Englewood Cliffs, 1992.

[44] M.A. Morris, M. Leboeuf, Kinetics of grain growth in a γ-based TiAl alloy, Scripta Mater. 38 (1998) 369–374.

[45] H.V. Atkinson, Theories of normal grain growth in pure single phase systems, Acta Metall. 36 (1988) 469–491.

[46] M. Hillert, Inhibition of grain growth by second-phase particles, Acta Metall. 36 (1988) 3177–3181.

[47] M.F. Ashby, J. Harper, J. Lewis, The interaction of crystal boundaries with second-phase particles, Trans. Met. Soc. AIME 245 (1969) 413–420.

[48] L. Priester, Grain boundaries: From theory to engineering, Springer, Dordrecht, 2013.

[49] P. Spoerk-Erdely, P. Staron, J. Liu, N. Kashaev, A. Stark, K. Hauschildt, E. Maawad, S. Mayer, H. Clemens, Exploring structural changes, manufacturing, joining, and repair of intermetallic γ-TiAl-based alloys: Recent progress enabled by in situ synchrotron X-ray techniques, Adv. Eng. Mater. (2021) 2000947.

[50] M. Musi, B. Galy, J.-P. Monchoux, A. Couret, H. Clemens, S. Mayer, In-situ observation of the phase evolution during an electromagnetic-assisted sintering experiment of an intermetallic γ-TiAl based alloy, Scripta Mater. 206 (2022) 114233.

[51] L.A. Yeoh, K.-D. Liss, A. Bartels, H. Chladil, M. Avdeev, H. Clemens, R. Gerling, T. Buslaps, In situ high-energy X-ray diffraction study and quantitative phase analysis in the α+γ phase field of titanium aluminides, Scripta Mater. 57 (2007) 1145–1148.

[52] D. Holec, R.K. Reddy, T. Klein, H. Clemens, Preferential site occupancy of alloying elements in TiAl-based phases, J. Appl. Phys. 119 (2016) 205104.

[53] M. Musi, P. Erdely, B. Rashkova, H. Clemens, A. Stark, P. Staron, N. Schell, S. Mayer, Evidence of an orthorhombic transition phase in a Ti-44Al-3Mo (at.%) alloy using in situ synchrotron diffraction and transmission electron microscopy, Mater. Char. 147 (2019) 398–405.

[54] B. Rashkova, K. Spiradek-Hahn, M. Brabetz, Z. Zhang, T. Schoeberl, H. Clemens, S. Mayer, Microstructural evolution and grain refinement in an intermetallic titanium aluminide alloy with a high molybdenum content, Int. J. Mat. Res. 106 (2015) 725–731.

[55] Y. Mishin, C. Herzig, Diffusion in the Ti–Al system, Acta Mater. 48 (2000) 589–623.

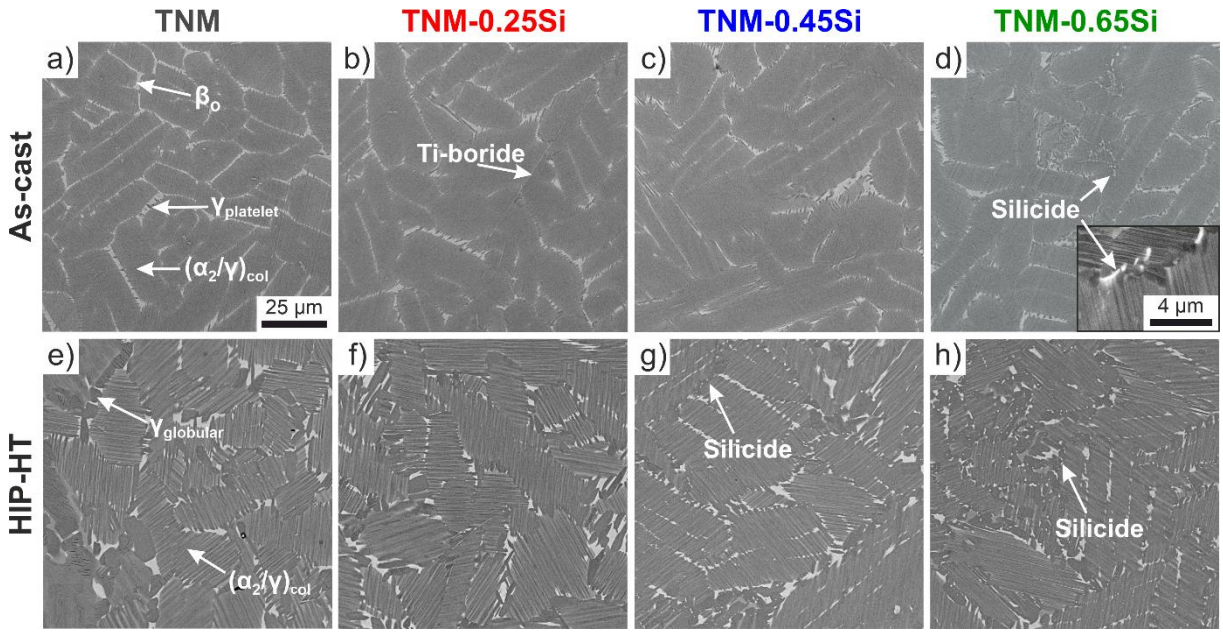

Fig. 1. SEM-BSE micrographs of the investigated alloys in the as-cast (a-d) and HIP heat-treated (e-h) material condition. Examples of individual microstructural constituents are marked. The contrasts of the phases are dark grey (γ), grey (α_2), light grey (β_o) and white (ζ-Ti_5Si_3 silicides). The insert in d) shows silicides at the boundary of lamellar α_2/γ colonies in the as-cast TNM-0.65Si alloy.

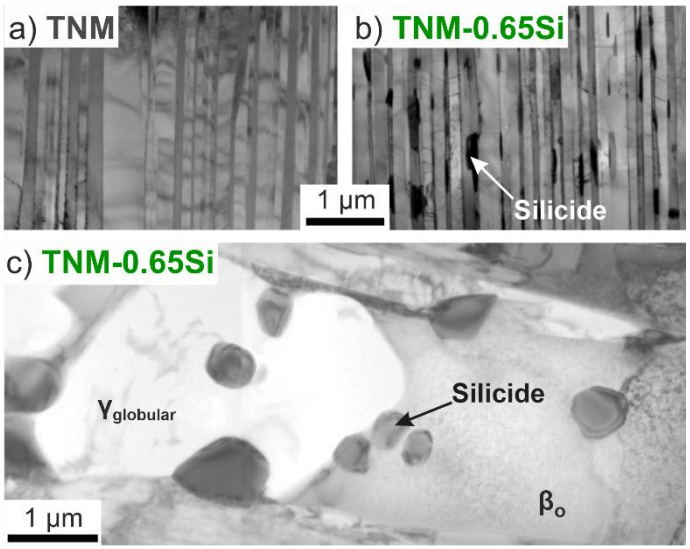

Fig. 2. TEM bright field images of different parts of the HIP heat-treated microstructure. In a) and b) lamellar α_2/γ colonies in the TNM and the TNM-0.65Si alloy, respectively, are shown; c) region between colonies in the TNM-0.65Si alloy containing globular γ phase, β_o phase and ζ-Ti_5Si_3 silicides. The individual phases were identified via selected area diffraction.

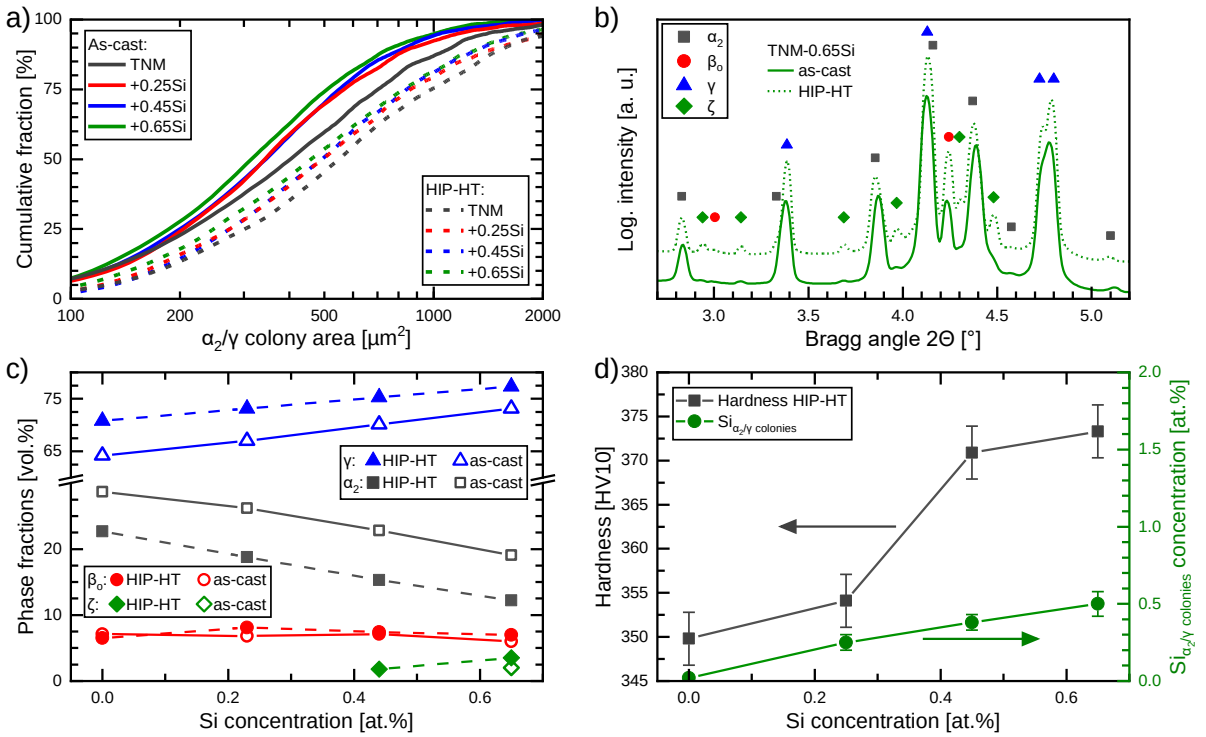

Fig. 3. a) Cumulative size distributions of the α_2/γ colonies in the as-cast (full lines) and HIP heat-treated (dashed lines) conditions; b) comparison of the room temperature HEXRD spectra of the TNM-0.65Si alloy in the as-cast (full line) and the HIP heat-treated (dotted line) condition. Peaks of the occurring phases are marked by individual symbols; c) phase fractions determined by ex-situ HEXRD as a function of the Si concentration for as-cast (full lines) and HIP heat-treated (dashed lines) material. The accuracy of the determined phase fractions is within ±2 vol.%; d) hardness (grey) and amount of Si dissolved in the α_2/γ colonies (green) in dependence of the alloys' total Si concentration.

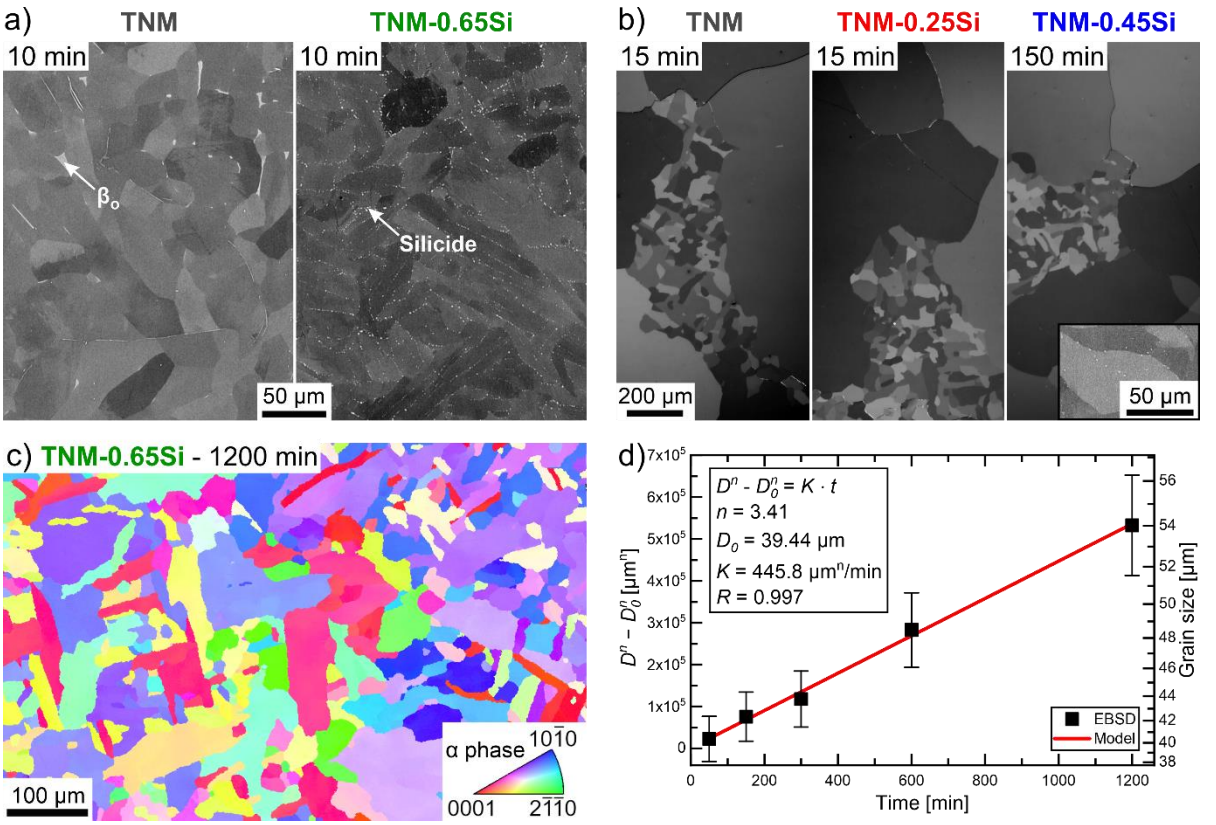

Fig. 4. Results of the grain coarsening study after heat treatments at 1300 °C; a) SEM-BSE images after a heat treatment time of 10 min for the TNM and TNM-0.65Si alloy; b) LOM micrographs showing discontinuous grain growth in the TNM (15 min), TNM-0.25Si (15 min) and the TNM-0.45Si (150 min) alloy; c) EBSD inverse pole figure map for TNM-0.65Si after 1200 min of heat treatment time; d) fit results of the theoretical model (red line) given by Eq. 1, with the size of the α grains (black symbols) determined by EBSD for several different heat treatment times.

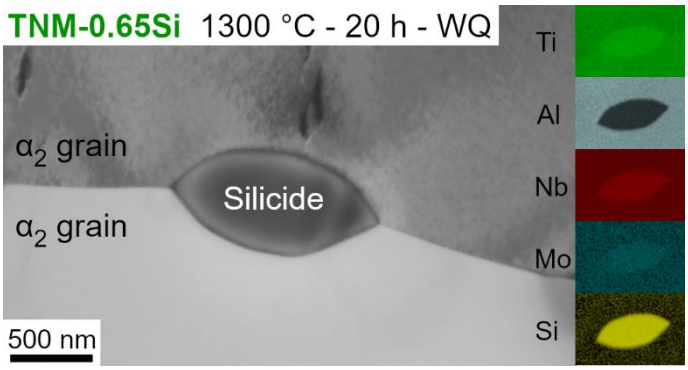

Fig. 5. TEM bright field micrograph of a ζ-Ti_5Si_3 silicide precipitate located at a grain boundary shared by two α_2 grains (α at high temperatures) in the TNM-0.65Si alloy after a heat treatment at 1300 °C for 20 h followed by water-quenching (WQ). Additionally, qualitative EDS maps for the elements Ti, Al, Nb, Mo, and Si are present.

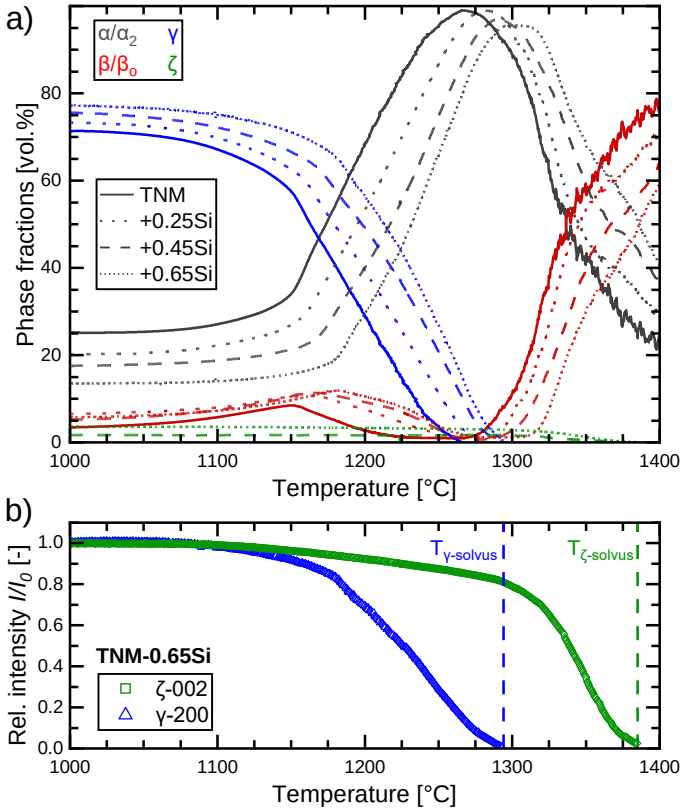

Fig. 6. a) Evolution of the volume fractions of α_2 (grey), β_o (red), γ (blue), and ζ-Ti_5Si_3 (green) for the TNM (full), TNM-0.25Si (short dashed), TNM-0.45Si (dashed), and TNM-0.65Si (dotted) alloy during in-situ HEXRD heating experiments; b) relative intensity evolution of the γ-200 peak (blue) and the ζ-Ti_5Si_3-002 peak (green) during the in-situ HEXRD heating experiment conducted on the TNM-0.65Si alloy. The intensity I_0 corresponds to the intensity of the respective peak at 1000 °C, i.e. at the start of the in-situ HEXRD heating experiments. The dissolution temperatures of the γ phase and the ζ-Ti_5Si_3 silicides are marked by individual lines.

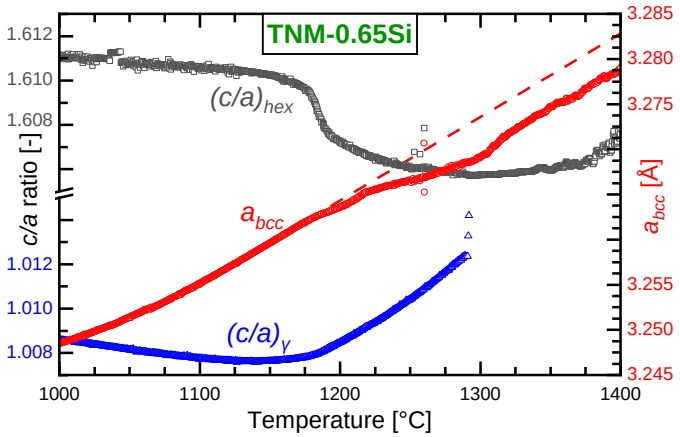

Fig. 7. Evolution of the *c/a* ratio of the α/α2 phase (c/a_{hex}, grey), the *c/a* ratio of the γ phase (c/a_{γ}, blue) and the lattice parameter of the β/β$_o$ phase (a_{bcc}, red) for the TNM-0.65Si alloy as determined by Rietveld analysis of the in-situ HEXRD data.

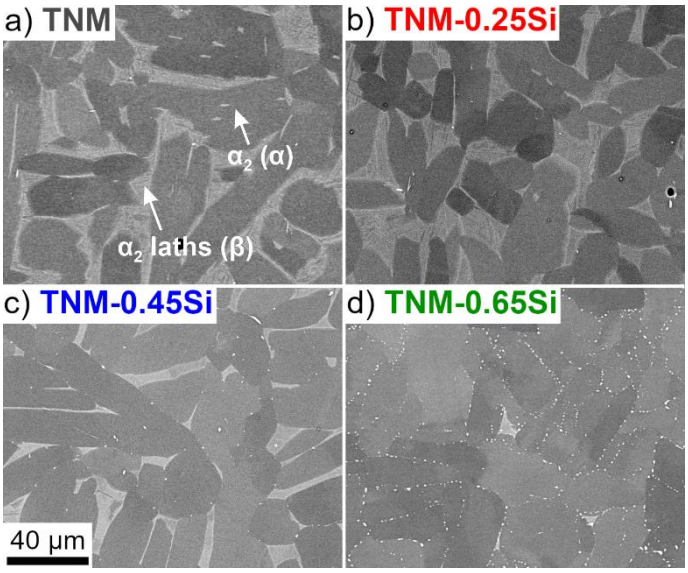

Fig. 8. SEM-BSE micrographs of the a) TNM, b) TNM-0.25Si, c) TNM-0.45Si, and d) TNM-0.65Si alloy after a heat treatment at 1300 °C for 1 h in a high-purity Ar atmosphere followed by quenching with Ar gas. The microstructural constituents α2 (high-temperature α phase) and α2 laths (high-temperature β phase) are marked by white arrows and their corresponding high-temperature counterparts are given in brackets.

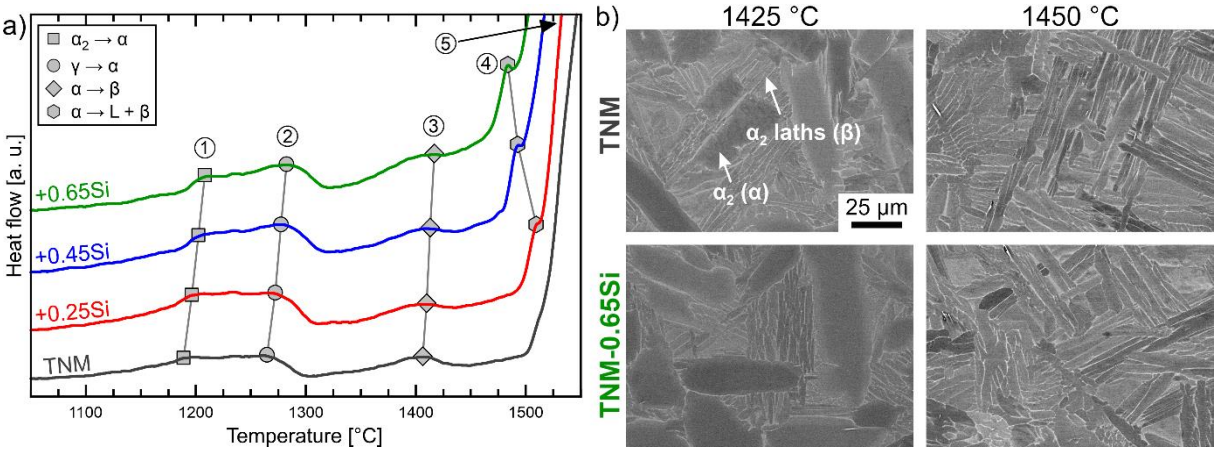

Fig. 9. a) DSC curves for a heating rate of 20 °C/min for the TNM (grey), TNM-0.25Si (red), TNM-0.45Si (blue) and TNM-0.65Si alloy (green). Peaks corresponding to phase transformations are marked by individual symbols and numbers: (1) eutectoid $\alpha_2 \rightarrow \alpha$, (2) $\gamma \rightarrow \alpha$, (3) $\alpha \rightarrow \beta$, (4) $\alpha \rightarrow L+\beta$, (5) solidus $\beta \rightarrow L$; b) SEM-BSE images of the TNM and TNM-0.65Si alloy after heat treatments at 1425 °C and 1450 °C for 30 min followed by water-quenching. The microstructural constituents α_2 (high-temperature α phase) and α_2 laths (high-temperature β phase) are marked by white arrows and their corresponding high-temperature counterparts are given in brackets.

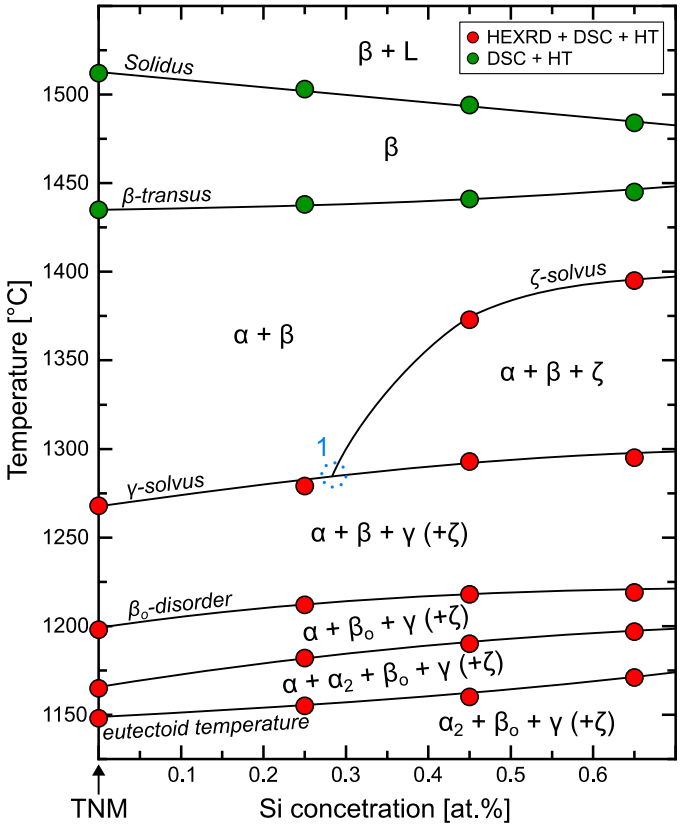

Fig. 10. Experimental quasi-binary phase diagram for TNM-based alloys in dependence of the Si content. Green points correspond to temperatures determined from DSC measurements with 20 °C/min as well as by means of heat treatments, while red points correspond to transformations determined by in-situ HEXRD, extrapolated DSC transformation temperatures and heat treatments. Circle 1 represents the lower boundary for the stability region of the ζ-Ti_5Si_3 silicides, see text.